


## Article

# An Integrated Electrochemical System for Synergistic Cathodic Nitrate Reduction and Anodic Sulfite Oxidation

Bing Cui <sup>1</sup>, Shizhao Wang <sup>1</sup>, Xiaofu Guo <sup>1</sup>, Yingying Zhao <sup>1,\*</sup> and Sohrab Rohani <sup>2,\*</sup> 

<sup>1</sup> Tianjin Key Laboratory of Chemical Process Safety, Hebei Collaborative Innovation Center of Modern Marine Chemical Technology, Engineering Research Center of Seawater Utilization of Ministry of Education, School of Chemical Engineering and Technology, Hebei University of Technology, Tianjin 300130, China; cuiqing23412@163.com (B.C.); shizhaow@163.com (S.W.); guoxiaofu@hebut.edu.cn (X.G.)

<sup>2</sup> Department of Chemical and Biochemical Engineering, Western University, London, ON N6A 5B9, Canada

\* Correspondence: luckyzhaoy@126.com (Y.Z.); srohani@uwo.ca (S.R.)

**Abstract:** Electrochemical reduction of nitrate has broad application prospects. However, in traditional electrochemical reduction of nitrate, the low value of oxygen produced by the anodic oxygen evolution reaction and the high overpotential limit its application. Seeking a more valuable and faster anodic reaction to form a cathode–anode integrated system with nitrate reaction can effectively accelerate the reaction rate of the cathode and anode, and improve the utilization of electrical energy. Sulfite, as a pollutant after wet desulfurization, has faster reaction kinetics in its oxidation reaction compared to the oxygen evolution reaction. Therefore, this study proposes an integrated cathodic nitrate reduction and anodic sulfite oxidation system. The effect of operating parameters (cathode potential, initial  $\text{NO}_3^-$ –N concentration, and initial  $\text{SO}_3^{2-}$ –S concentration) on the integrated system was studied. Under the optimal operating parameters, the nitrate reduction rate in the integrated system reached 93.26% within 1 h, and the sulfite oxidation rate reached 94.64%. Compared with the nitrate reduction rate (91.26%) and sulfite oxidation rate (53.33%) in the separate system, the integrated system had a significant synergistic effect. This work provides a reference for solving nitrate and sulfite pollution, and promotes the application and development of electrochemical cathode–anode integrated technology.

**Keywords:** electrochemical; integrated system; nitrate reduction; sulfite oxidation



**Citation:** Cui, B.; Wang, S.; Guo, X.; Zhao, Y.; Rohani, S. An Integrated Electrochemical System for Synergistic Cathodic Nitrate Reduction and Anodic Sulfite Oxidation. *Molecules* **2023**, *28*, 4666. <https://doi.org/10.3390/molecules28124666>

Academic Editor: Ioannis V. Yentekakis

Received: 17 May 2023

Revised: 7 June 2023

Accepted: 7 June 2023

Published: 9 June 2023



**Copyright:** © 2023 by the authors. Licensee MDPI, Basel, Switzerland. This article is an open access article distributed under the terms and conditions of the Creative Commons Attribution (CC BY) license (<https://creativecommons.org/licenses/by/4.0/>).

## 1. Introduction

In recent years, accelerated industrialization and increasing human activities have led to severe nitrate pollution [1]. Compared with other techniques, such as biological and adsorption methods, the electrochemical reduction of nitrate technology has the advantages of fast removal rate, low cost, and no chemical additives [2–4]. It can directly convert harmful nitrate into valuable ammonia, making it a promising nitrate treatment technology. In the traditional electrochemical reduction of nitrate process, the anodic half-reaction is the oxygen evolution reaction (OER), and the economic value of oxygen is limited, so it is usually directly released into the air. In addition, the occurrence of OER requires a high overpotential, which to some extent limits the nitrate reduction rate and causes energy waste [5]. Up to now, researchers have always been keen to develop new materials to obtain higher nitrate reduction rates and product selectivity in exploring the electrochemical reduction of nitrate, and there is almost no research focusing on the application of anodic reactions.

Seeking more valuable anodic reactions to match with nitrate reduction reactions to form an integrated cathodic reduction–anodic oxidation system is highly desirable. In contrast to a single anode or cathode reaction, the integrated cathode reduction–anode oxidation system simultaneously focuses on the anode and cathode reactions, achieving matching reaction rates in a unit system [6]. As a result, the electrochemical cathode–anode integrated

system has significant advantages: (1) the matching reaction between the cathode and anode synergistically improves the reaction rates; (2) integrated cathode–anode can simultaneously treat two systems, significantly reducing process costs; and (3) cathode–anode coupling replaces the hydrogen evolution reaction (HER) and oxygen evolution reaction (OER) in separate oxidation and reduction processes, improving energy utilization efficiency [7–9].

Sulfite is the main product after wet desulfurization; excess sulfite will cause water and soil pollution, decomposition will release  $\text{SO}_2$  again, and timely oxidation of sulfite to sulfate can effectively avoid secondary pollution [10,11]. Compared to OER, the oxidation reaction of sulfite (SOR) generated in the desulfurization process exhibits faster kinetics [9,12]. Therefore, by combining cathodic nitrate reduction with anodic sulfite oxidation through electrochemical reactions, synergistic efficiency can be achieved in treating wastewater containing nitrate and sulfite.

In this study, the anodic sulfite oxidation reaction (SOR) was employed to replace the OER, and an electrochemical system integrating cathodic  $\text{NO}_3^-$  RR with anodic SOR was constructed for the synergistic treatment of both wastewaters. The optimal treatment conditions of the coupled system were determined by investigating the influencing factors including the cathodic potential, initial nitrate concentration, and initial sulfite concentration. The development of this integrated system could provide valuable insights into the development and applications of synergistic electrochemical technology.

## 2. Results and Discussion

### 2.1. Characterizations of $\text{CuO}\&\text{Cu}_2\text{O}@C$ Electrode

The physical phases of the constructed electrode were analyzed via XRD. Figure 1a shows the electrode as a mixed composition of CuO (JCPDS No. 78–2076) and  $\text{Cu}_2\text{O}$  (JCPDS No. 89–2529). The strong diffraction peaks at  $36.4^\circ$  and  $42.3^\circ$  are attributed to the (1 1 1) and (2 0 0) crystal planes of  $\text{Cu}_2\text{O}$ . The characteristic diffraction peaks at  $35.6^\circ$ ,  $38.7^\circ$ ,  $48.8^\circ$ , and  $58.2^\circ$  are associated with the (–1 1 1) (1 1 1) (–2 0 2) (2 0 0) crystalline plane of CuO. SEM characterization was used to analyze the surface morphology of the prepared electrode. As shown in Figure 1b,c, the surface of the CC substrate material was uncontaminated, and the constructed electrode surface formed uniform nanoparticles. In order to further clarify the composition and microstructure of the surface nanoparticles, TEM characterization was performed. The TEM image in Figure 1d further shows that nanoparticles were forming on the CC surface. In the HRTEM image (Figure 1e–i), the lattice spacing of the stripes with 0.211 nm, 0.247 nm, and 0.232 nm is attributed to the (2 0 0) and (1 1 1) crystal faces of  $\text{Cu}_2\text{O}$  and the (1 1 1) crystal face of CuO [13,14], respectively. This is consistent with the XRD results and fully demonstrates that the composition of the nanoparticles formed on the electrode surface is CuO and  $\text{Cu}_2\text{O}$ .

In order to gain a deeper understanding of the nanoparticles on the electrode surface, the element composition and related valence states of the electrode were analyzed via XPS characterization. The XPS full spectrum (Figure 2a) shows the presence of Cu and O elements on the electrode surface, further proving the existence of Cu-related species on the electrode surface. As shown in Figure 2b, the high-resolution C1s spectrum was deconvoluted into three peaks, which could be assigned as C=C/C–C (284.8 eV), C–O (285.6 eV), and C=O (288.4 eV), respectively [13]. The high-resolution Cu 2p spectrum (Figure 2c) contains characteristic peaks of Cu(I) and Cu(II). The peaks at 933.8 eV and 953.6 eV are attributed to the Cu 2p<sub>3/2</sub> and Cu 2p<sub>1/2</sub> of  $\text{Cu}_2\text{O}$ , respectively [15]. A clear satellite peak appears near the peaks at 935.4 eV and 955.1 eV, which is a typical feature of Cu(II) [16]. The high-resolution O 1s spectra (Figure 2d) can be deconvoluted into two peaks, which are hydroxyl oxygen (–OH, 531.7 eV) and lattice oxygen ( $\text{O}_{\text{latt}}$ , 530.1 eV) [17]. The XPS results are consistent with the TEM results, further proving the synthesis of the  $\text{CuO}\&\text{Cu}_2\text{O}@C$  electrode.

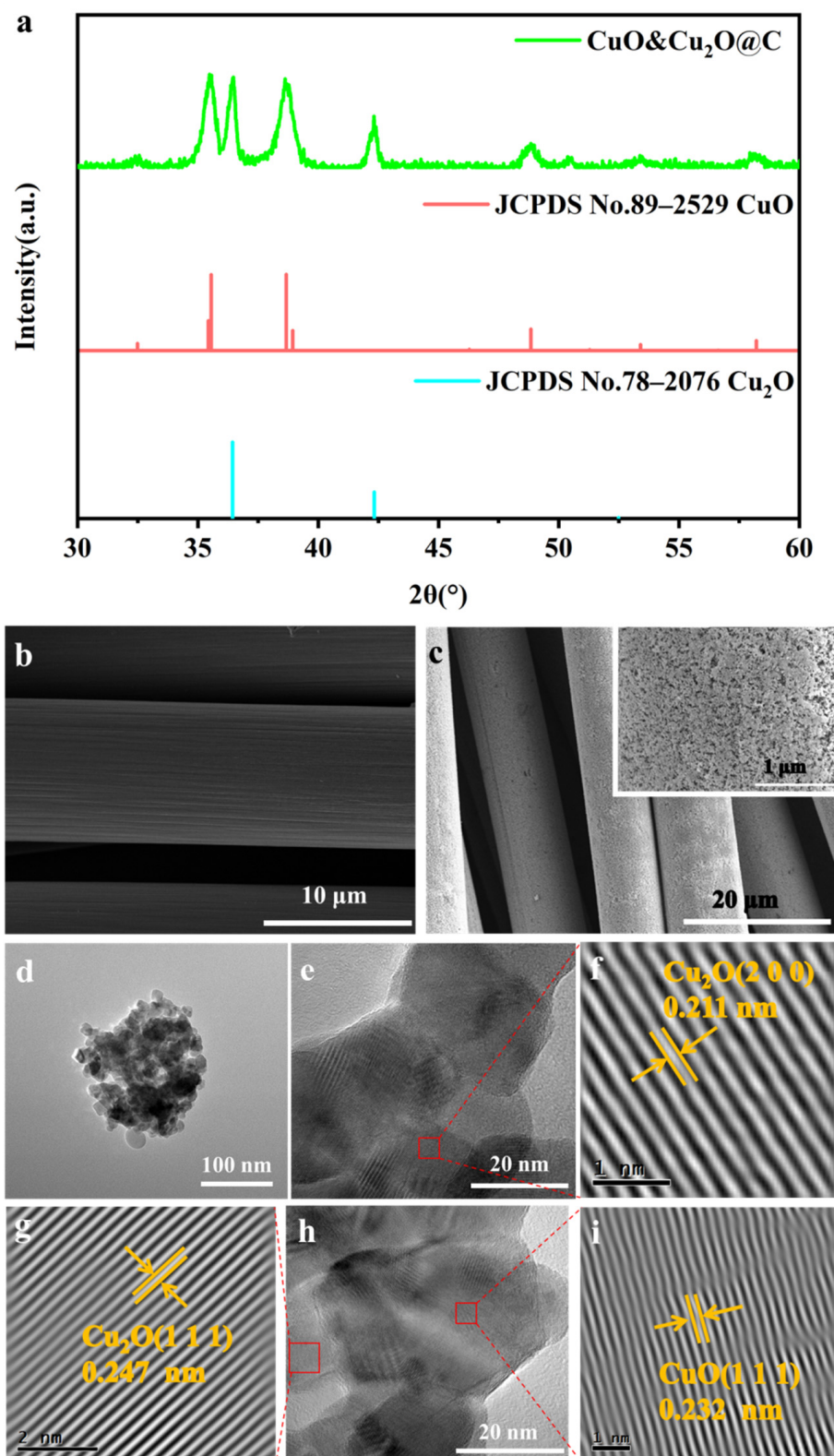


**Figure 1.** (a) XRD patterns of CuO&Cu<sub>2</sub>O@C; (b) SEM image of CC; (c) SEM images of CuO&Cu<sub>2</sub>O@C; (d) TEM image; (e–i) HRTEM images of CuO&Cu<sub>2</sub>O@C.

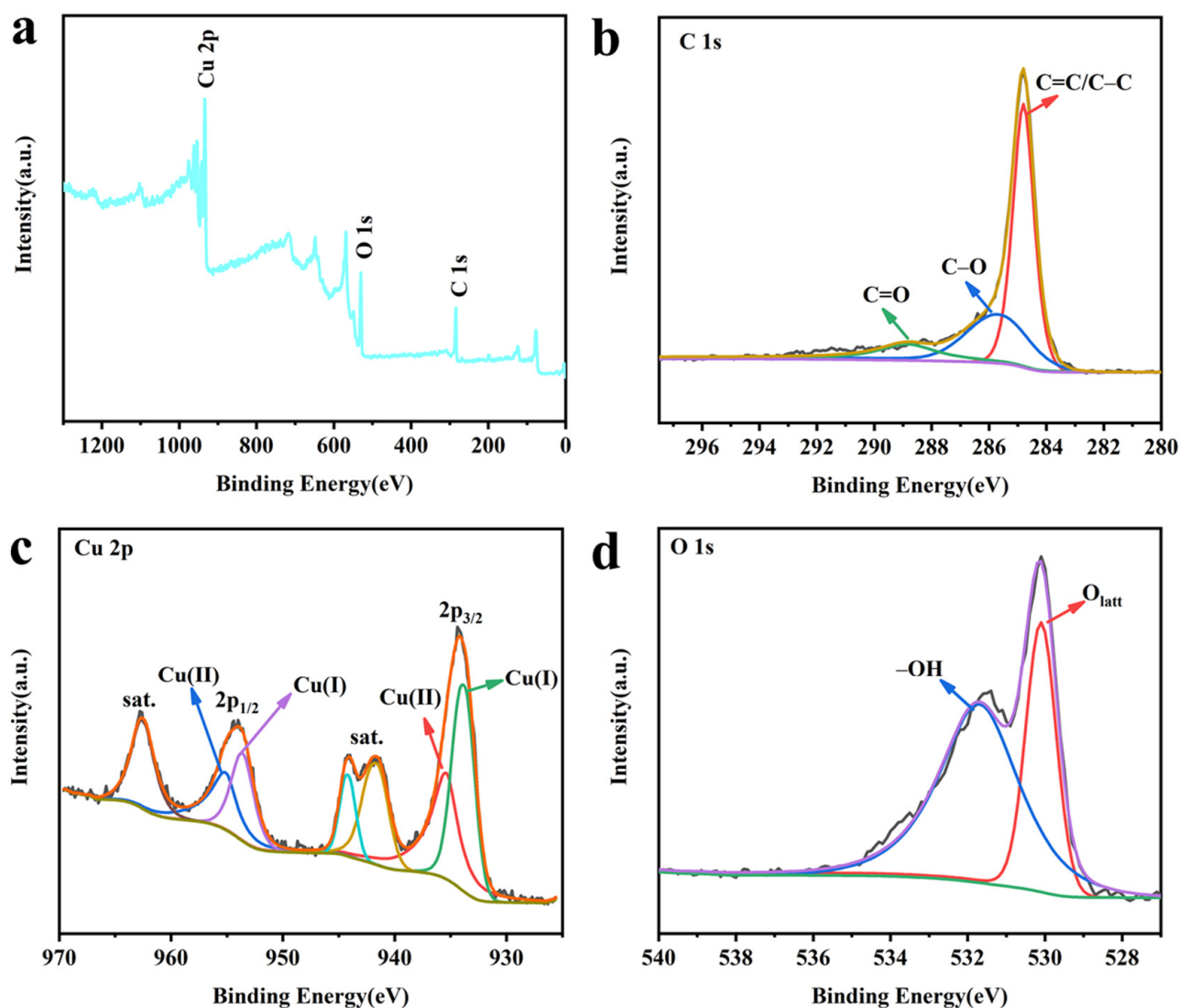


**Figure 2.** (a) XPS full-range spectra; (b) high-resolution Cu 1s; (c) high-resolution Cu 2p; (d) high-resolution O 1s of CuO&Cu<sub>2</sub>O@C.

## 2.2. Electrochemical Reduction of Nitrate

After confirming the structure of the CuO&Cu<sub>2</sub>O@C electrode, the nitrate reduction activity of this electrode was investigated using different cathodic potentials. Figure 3a shows a significant decay trend of nitrate concentration within 60 min under different potentials, indicating that CuO/Cu<sub>2</sub>O@C electrode can effectively reduce nitrate. As the potential increases from  $-1.2$  V to  $-1.8$  V, the removal rate shows a volcano-like change. When applying  $-1.2$  V cathodic potential, the removal rate is the lowest, at only 51.59%. This is because at a lower potential, there are not enough electrons provided to reduce nitrate [18]. As the cathodic potential further increases to  $-1.4$  V, the nitrate removal rate increases to 91.61%. This is because the increase in the cathodic potential results in an increase in the amount of electron transfer in the system. When the cathodic potential becomes more negative than  $-1.4$  V, the competitive hydrogen evolution reaction gradually increases, leading to the inhibition of nitrate reduction reaction and a gradual decrease in the removal rate [19]. In order to evaluate the rate of electrochemical reduction of nitrate, the nitrate reduction process was fitted with a pseudo-first-order kinetic model, and the result is shown in Figure S1.  $R^2$  indicates that the nitrate reduction conforms to the pseudo-first-order kinetic model and has the fastest reaction rate at  $-1.4$  V, with a kinetic constant ( $k_r$ ) of  $2.4386 \text{ h}^{-1}$ .

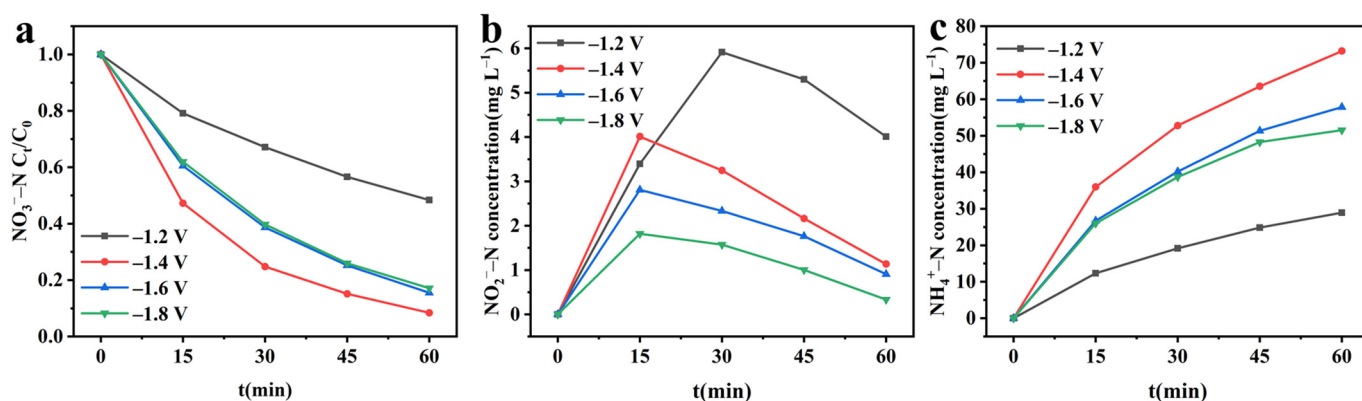


**Figure 3.** Electrochemical reduction of nitrate at different cathodic potentials. (a)  $\text{NO}_3^-$ -N concentration; (b)  $\text{NO}_2^-$ -N concentration; (c)  $\text{NH}_4^+$ -N concentration.

To investigate the reduction products of nitrate, the concentration changes of  $\text{NO}_2^-$ -N and  $\text{NH}_4^+$ -N were continuously detected. In the early stage of the reaction, the concentrations of both  $\text{NO}_2^-$ -N and  $\text{NH}_4^+$ -N showed an increasing trend. However, in the later stages of the reaction, the concentration of  $\text{NO}_2^-$ -N showed a decreasing trend, while  $\text{NH}_4^+$ -N continued to increase (Figure 3b,c). This indicates that  $\text{NO}_2^-$ -N is the intermediate product of  $\text{NO}_3^-$ -N reduction, and  $\text{NH}_4^+$ -N is the final product of nitrate reduction [20]. The cumulative amount of  $\text{NH}_4^+$ -N increases with the increase of cathodic potential, which is consistent with the change law of nitrate removal rate, and also shows a volcano-like shape. This is because the decay of nitrate determines the generation of the final product  $\text{NH}_4^+$ -N. At high nitrate removal rates, it allows more  $\text{NO}_3^-$ -N to be converted to  $\text{NH}_4^+$ -N.

### 2.3. Self-Oxidation and Anodic Electro-Oxidation of Sulfite

To investigate the electro-oxidation performance of  $\text{SO}_3^{2-}$ -S on a Pt sheet electrode, a separate study of the electrochemical oxidation of sulfite was conducted, and self-oxidation experiments were conducted to eliminate the effect of air on sulfite oxidation. As shown in Figure 4, the  $\text{SO}_3^{2-}$ -S concentration remained essentially constant during the self-oxidation, indicating that  $\text{SO}_3^{2-}$ -S was not oxidized by air in the H-type sealed electrolytic cell. In addition, the oxidation of  $\text{SO}_3^{2-}$ -S was all electrically driven during the electro-oxidation process. As the cathodic potential increased from  $-1.2$  V to  $-1.8$  V, the oxidation rate of  $\text{SO}_3^{2-}$ -S increased from 13.5% to 100%; moreover, the oxidation was complete within 45 min at  $-1.8$  V. This demonstrates that the Pt electrode possessed effective  $\text{SO}_3^{2-}$ -S oxidization capability. The electro-oxidation process was fitted with a pseudo-first-order kinetic model, and the kinetic constants obtained for different cathodic potentials indicated that the electro-oxidation process of  $\text{SO}_3^{2-}$ -S conforms to the pseudo-first-order kinetic process (Figure S2). As the cathodic potential increases, the kinetic constant of the electro-oxidation process of  $\text{SO}_3^{2-}$ -S also increases, which is because at higher potentials, more electrons are generated, thereby accelerating the reaction rate [21].

### 2.4. Integrated Electrochemical System

Based on the single system of electrochemical reduction of nitrate and sulfite oxidation, the two were paired to construct an integrated system to achieve simultaneous treatment of nitrate and sulfite.

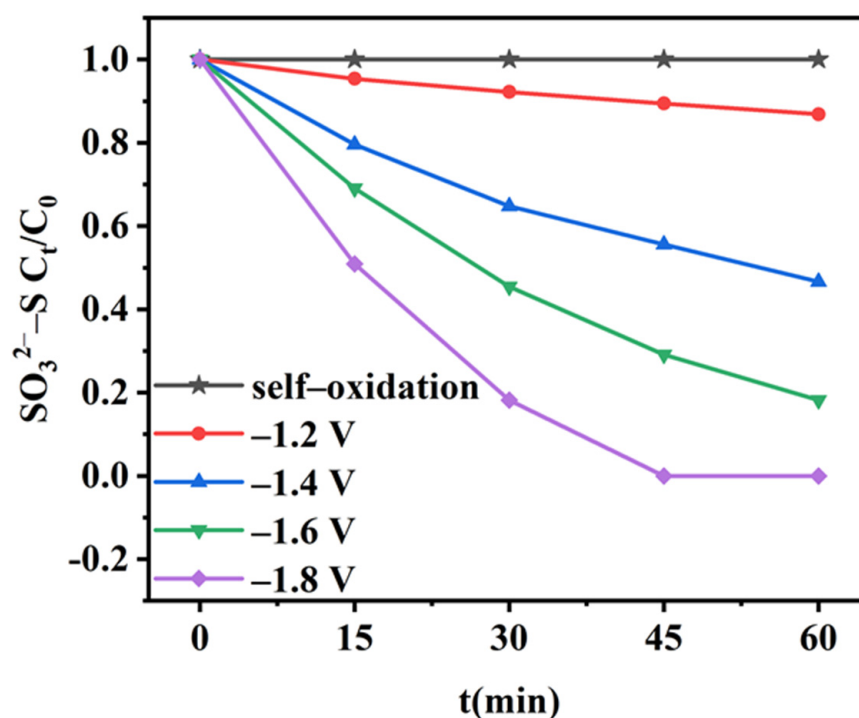


**Figure 4.**  $\text{SO}_3^{2-}\text{-S}$  concentration during self-oxidation and electro-oxidation at different potentials.

#### 2.4.1. Effect of the Applied Cathode Potentials

In electrochemical reactions, electrode potential plays a crucial role; therefore, the effect of cathode potential on the integrated system was explored. As shown in Figure 5a, in the integrated system, as the cathode potential increases from  $-1.2$  V to  $-1.4$  V, the  $\text{NO}_3^-$ -N removal rate increases from 56.28% to 93.26%. Continuing to improve the cathode potential to  $-1.8$  V, the removal rate remains above 90%. The pseudo-first-order kinetic model fitting results for  $\text{NO}_3^-$ -N reduction (Figure S3a) indicate that  $\text{NO}_3^-$ -N reduction in the integrated system still belongs to the pseudo-first-order kinetic process. The reaction kinetic constant is highest at a cathode potential of  $-1.4$  V, reaching  $2.6622 \text{ h}^{-1}$ . Figure 5b,c shows the changes in the products  $\text{NO}_2^-$ -N and  $\text{NH}_4^+$ -N in the integrated system at different potentials. The accumulation of  $\text{NO}_2^-$ -N remains at a low level of  $5 \text{ mg L}^{-1}$  for 1 h at different potentials. The accumulation of  $\text{NH}_4^+$ -N increases first and then decreases with the increase of potential, and the highest accumulation was  $-1.4$  V. The reason for the above phenomenon is consistent with that in the single reduction system. At lower potentials, the insufficient electrons produced eventuate  $\text{NO}_3^-$ -N removal, while at higher potentials, a large amount of hydrogen evolution reaction becomes the primary reaction, hindering the conversion of  $\text{NO}_3^-$ -N [22]. As shown in Figure 5d, with the increase of cathode potential, the oxidation rate of  $\text{SO}_3^{2-}\text{-S}$  in the integrated system increases from 64.91% to 100%. As shown in Figure S3b, the oxidation of  $\text{SO}_3^{2-}\text{-S}$  in the integrated system is also a pseudo-first-order kinetic process.

Table 1 shows the comparison of performance parameters between single electrochemical systems and integrated electrochemical systems. In the integrated system, the removal rate of  $\text{NO}_3^-$ -N and the oxidation rate of  $\text{SO}_3^{2-}\text{-S}$  are both improved at different cathode potentials. This implies that the constructed integrated system has synergistic effects. This is because in the single  $\text{NO}_3^-$ -N reduction system, the anode reaction is oxygen evolution, while in the integrated system, the anode reaction is  $\text{SO}_3^{2-}\text{-S}$  oxidation, which has lower activation energy and only requires two electrons to complete the reaction, while the oxygen evolution reaction has higher activation energy and requires four electrons. As a result, the oxidation reaction rate  $\text{SO}_3^{2-}\text{-S}$  is faster in the integrated system, making for a higher reaction current, which promotes the reduction of  $\text{NO}_3^-$ -N [12]. As for the single sulfite

reaction system, the cathode is hydrogen evolution reaction, and the hydrogen evolution reaction rate of the prepared CuO&Cu<sub>2</sub>O@C electrode is slow. However, in the integrated system, the CuO&Cu<sub>2</sub>O@C electrode accelerates the reduction rate of NO<sub>3</sub><sup>−</sup>-N, and thus elevates the ability of the anode to oxidize SO<sub>3</sub><sup>2−</sup>-S. It is worth noting that the enhancement amplitude of NO<sub>3</sub><sup>−</sup>-N removal is low at lower potentials of −1.2 V and −1.4 V, while it is significant at higher potentials of −1.6 V and −1.8 V. This is because at high negative potentials, a large amount of hydrogen evolution reaction occurs in the single reduction system, which inhibits the reduction of NO<sub>3</sub><sup>−</sup>-N, while at low potentials, the hydrogen evolution reaction does not occur violently [23]. In the integrated system, SO<sub>3</sub><sup>2−</sup>-S oxidation inhibits the occurrence of hydrogen evolution reaction [24], and therefore the magnitude of the potentiation varies at different potentials. In addition, the increase of NH<sub>4</sub><sup>+</sup>-N selectivity at different potentials is consistent with the pattern of NO<sub>3</sub><sup>−</sup>-RR increase. This is due to the fact that NO<sub>3</sub><sup>−</sup>-RR is directly related to the formation of the final product NH<sub>4</sub><sup>+</sup>-N [25].

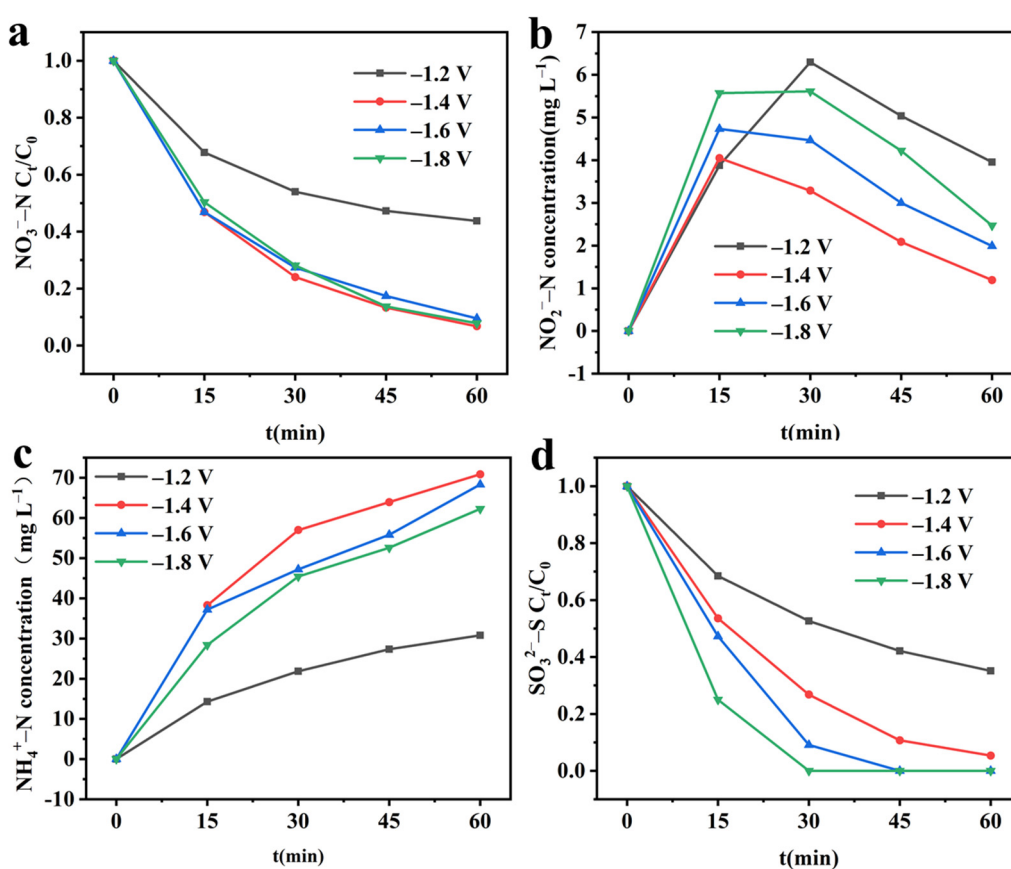


**Figure 5.** Effect of cathodic potential on the performance of integrated electrochemical systems. (a) NO<sub>3</sub><sup>−</sup>-N concentration; (b) NO<sub>2</sub><sup>−</sup>-N concentration; (c) NH<sub>4</sub><sup>+</sup>-N concentration; (d) SO<sub>3</sub><sup>2−</sup>-S concentration. Experimental conditions: initial NO<sub>3</sub><sup>−</sup>-N concentration = 100 mg L<sup>−1</sup>; initial SO<sub>3</sub><sup>2−</sup>-S concentration = 1.0 g L<sup>−1</sup>.

**Table 1.** Comparison of single system and integrated system performance parameters.

	R (NO <sub>3</sub> <sup>−</sup> -N)/%		S (NO <sub>2</sub> <sup>−</sup> -N)/%		S (NH <sub>4</sub> <sup>+</sup> -N)/%		O (SO <sub>3</sub> <sup>2−</sup> -S)/%	
	Single	Integrated	Single	Integrated	Single	Integrate	Single	Integrated
−1.2 V	51.59	56.28	7.64	6.80	55.14	53.50	13.15	64.91
−1.4 V	91.61	93.26	1.22	1.25	78.41	74.90	53.33	94.64
−1.6 V	84.46	90.46	1.05	2.10	67.21	73.20	81.82	100.00
−1.8 V	82.89	92.19	0.40	2.60	61.39	66.70	100.00	100.00

By comparing various performance indicators, it can be seen that the  $\text{NO}_3^-$ -N removal rate is optimal at  $-1.4$  V, the  $\text{NO}_2^-$ -N selectivity is the lowest, the  $\text{NH}_4^+$ -N selectivity is the highest, and although the  $\text{SO}_3^{2-}$ -S oxidation rate is not the highest, it still exhibits excellent performance. Therefore, it was reasonable to choose  $-1.4$  V for the subsequent experiments.

#### 2.4.2. Effect of Initial $\text{NO}_3^-$ -N Concentration

In integrated electrochemical systems, changes in the half-reaction rate can affect the overall system reaction rate [26]. Changes in the initial  $\text{NO}_3^-$ -N concentration affect the cathodic reaction  $\text{NO}_3^-$ -RR rate [27], so the effect of different initial  $\text{NO}_3^-$ -N concentrations on the integrated system was investigated. As shown in Figure 6a and Figure S4a, as the initial  $\text{NO}_3^-$ -N concentration increases from  $50 \text{ mg L}^{-1}$  to  $100 \text{ mg L}^{-1}$ , the  $\text{NO}_3^-$ -N removal rate first increases and reaches a maximum of 93.26% at  $100 \text{ mg L}^{-1}$ , with the fastest reaction rate. As the initial  $\text{NO}_3^-$ -N concentration continues to increase, the  $\text{NO}_3^-$ -N removal rate continues to decrease, with the lowest removal rate at  $250 \text{ mg L}^{-1}$ , only 46.91%, and the slowest reaction rate. The lower removal rate at a low initial  $\text{NO}_3^-$ -N concentration is due to the limited binding capacity of  $\text{NO}_3^-$ -N, which leads to a decrease in the effective collision frequency of active molecules [28]. At higher concentrations, the lower  $\text{NO}_3^-$ -N removal rate is due to the limited catalytic active sites on the  $\text{CuO}\&\text{Cu}_2\text{O}\&\text{C}$  electrode surface [29]. As shown in Figure 6b,c, with the increase of initial  $\text{NO}_3^-$ -N concentration, the selectivity of  $\text{NO}_2^-$ -N first increases and then decreases, while the selectivity of  $\text{NH}_4^+$ -N shows the opposite trend. This is because at low initial  $\text{NO}_3^-$ -N concentrations, the rate of conversion of  $\text{NO}_3^-$ -N to the intermediate product  $\text{NO}_2^-$ -N is lower than the rate of conversion of  $\text{NO}_2^-$ -N to  $\text{NH}_4^+$ -N, while at higher initial  $\text{NO}_3^-$ -N concentrations, the rate of conversion of  $\text{NO}_3^-$ -N to the intermediate product  $\text{NO}_2^-$ -N is higher than the rate of conversion of  $\text{NO}_2^-$ -N to  $\text{NH}_4^+$ -N.

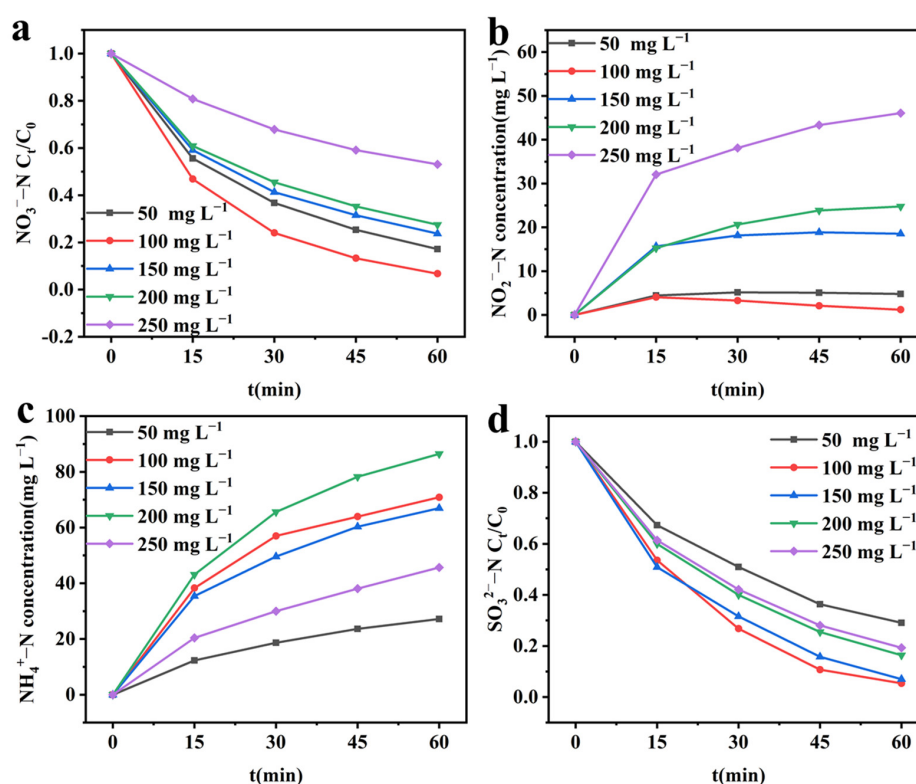


**Figure 6.** Effect of initial  $\text{NO}_3^-$ -N concentration on the performance of integrated electrochemical systems. (a)  $\text{NO}_3^-$ -N concentration; (b)  $\text{NO}_2^-$ -N concentration; (c)  $\text{NH}_4^+$ -N concentration; (d)  $\text{SO}_3^{2-}$ -S concentration. Experimental conditions: cathodic potential =  $-1.4$  V; initial  $\text{SO}_3^{2-}$ -S concentration =  $1.0 \text{ g L}^{-1}$ .



As shown in Figure 6d, as the initial  $\text{NO}_3^-$ -N concentration increases from  $50 \text{ mg L}^{-1}$  to  $100 \text{ mg L}^{-1}$ , the  $\text{SO}_3^{2-}$ -S oxidation rate increases from 70.91% to 94.64%. As the initial  $\text{NO}_3^-$ -N concentration further increases, the  $\text{SO}_3^{2-}$ -S oxidation rate gradually decreases and decreases to 80.70% at  $250 \text{ mg L}^{-1}$ . As shown in Figure S4b, the oxidation kinetic constant  $k_o$  first increases and then decreases with the rise in initial  $\text{NO}_3^-$ -N concentration, which is consistent with the changing trend of cathodic reduction  $\text{NO}_3^-$ -N kinetic constant. This indicates that the change in the cathodic reaction rate will cause the same change trend in the anodic reaction rate, which is due to the mutual matching relationship between the cathodic and anodic reaction rates. When the rates of the two half-reactions do not match, they will decrease simultaneously.

By comparing the  $\text{NO}_3^-$ -N reduction rate,  $\text{SO}_3^{2-}$ -S oxidation rate,  $\text{NO}_2^-$ -N selectivity, and  $\text{NH}_4^+$ -N selectivity, it is easy to find that the initial  $\text{NO}_3^-$ -N concentration of  $100 \text{ mg L}^{-1}$  showed excellent performance in all the above indexes, so it was chosen as the initial  $\text{NO}_3^-$ -N concentration for the subsequent study.

#### 2.4.3. Effect of Initial $\text{SO}_3^{2-}$ -S Concentration on Integrated Electrochemical System

The initial  $\text{SO}_3^{2-}$ -S concentration in the anode chamber is closely related to the SOR rate [30], which affects the cathodic reaction rate. Based on this, the effect of initial  $\text{SO}_3^{2-}$ -S concentration on the integrated system was investigated. As shown in Figure 7a, as the initial  $\text{SO}_3^{2-}$ -S concentration increases from  $0.4 \text{ g L}^{-1}$  to  $1.0 \text{ g L}^{-1}$ , the  $\text{SO}_3^{2-}$ -S oxidation rate increases continuously from 80.00% to 94.64%. When the initial  $\text{SO}_3^{2-}$ -S concentration is further increased to  $1.2 \text{ g L}^{-1}$ , the  $\text{SO}_3^{2-}$ -S oxidation rate decreases to 90.91%. As the initial  $\text{SO}_3^{2-}$ -S concentration increases, the oxidation kinetic constant  $k_o$  shows a trend of first increasing and then declining (Figure S5a). At concentrations of 0.4, 0.6, 0.8, 1.0, and  $1.2 \text{ g L}^{-1}$ , the reduction rates of  $\text{NO}_3^-$ -N are 80.51%, 84.42%, 87.80%, 93.26%, and 86.37%, respectively (Figure 7b). The fitting results of cathodic reduction  $\text{NO}_3^-$ -N to first-order kinetics show (Figure S5b) that as the initial  $\text{SO}_3^{2-}$ -S concentration continuously increases,  $k_r$  increases from  $1.5891 \text{ h}^{-1}$  to  $2.6622 \text{ h}^{-1}$  and then decreases to  $1.9384 \text{ h}^{-1}$ . This changing trend is consistent with the  $\text{SO}_3^{2-}$ -S oxidation kinetic constant trend. This once again indicates that at lower initial  $\text{SO}_3^{2-}$ -S concentration, the anodic oxidation reaction cannot match the cathodic reduction reaction, resulting in a decrease in the cathodic and anodic reaction rates in the integrated system. As the initial  $\text{SO}_3^{2-}$ -S concentration increases, the anodic and cathodic reactions gradually match, resulting in the highest rates of sulfite oxidation and nitrate reduction at an initial  $\text{SO}_3^{2-}$ -S concentration of  $1.0 \text{ g L}^{-1}$ . When the initial  $\text{SO}_3^{2-}$ -S concentration continues to increase to  $1.2 \text{ g L}^{-1}$ , this mismatch reappears, resulting in a decrease in the performance of the integrated system.

Figure 7c,d shows the changes of the products  $\text{NO}_2^-$ -N and  $\text{NH}_4^+$ -N at different initial  $\text{SO}_3^{2-}$ -S concentrations, respectively. The accumulation of  $\text{NO}_2^-$ -N first decreased with the increase of initial  $\text{SO}_3^{2-}$ -S concentration, reaching a minimum at  $1.0 \text{ g L}^{-1}$ , and then increased with the further increase in  $\text{SO}_3^{2-}$ -S concentrations. The  $\text{NH}_4^+$ -N production showed a trend of increasing and then decreasing, with the highest production at the initial  $\text{SO}_3^{2-}$ -S concentration of  $1.0 \text{ g L}^{-1}$ . This indicates that the decrease in the reaction rate during the cathodic reduction of nitrate leads to the accumulation of intermediate products, affecting the transformation of intermediate products to final products.

In this system,  $\text{NO}_3^-$  is converted to  $\text{NH}_4^+$  at the cathode and  $\text{SO}_3^{2-}$  is converted to  $\text{SO}_4^{2-}$  at the anode. The final products could be recycled via crystallization and utilized to form valuable compounds such as magnesium ammonia phosphate (struvite precipitate,  $\text{NH}_4\text{MgPO}_4 \cdot 6\text{H}_2\text{O}$ ) [31,32], calcium sulfate ( $\text{CaSO}_4$ ), barium sulfate ( $\text{BaSO}_4$ ), Ettringite ( $\text{Ca}_6\text{Al}_2(\text{SO}_4)_3(\text{OH})_{12}$ ) [33], etc., thus achieving more effective treatment of nitrate and sulfite in wastewater.

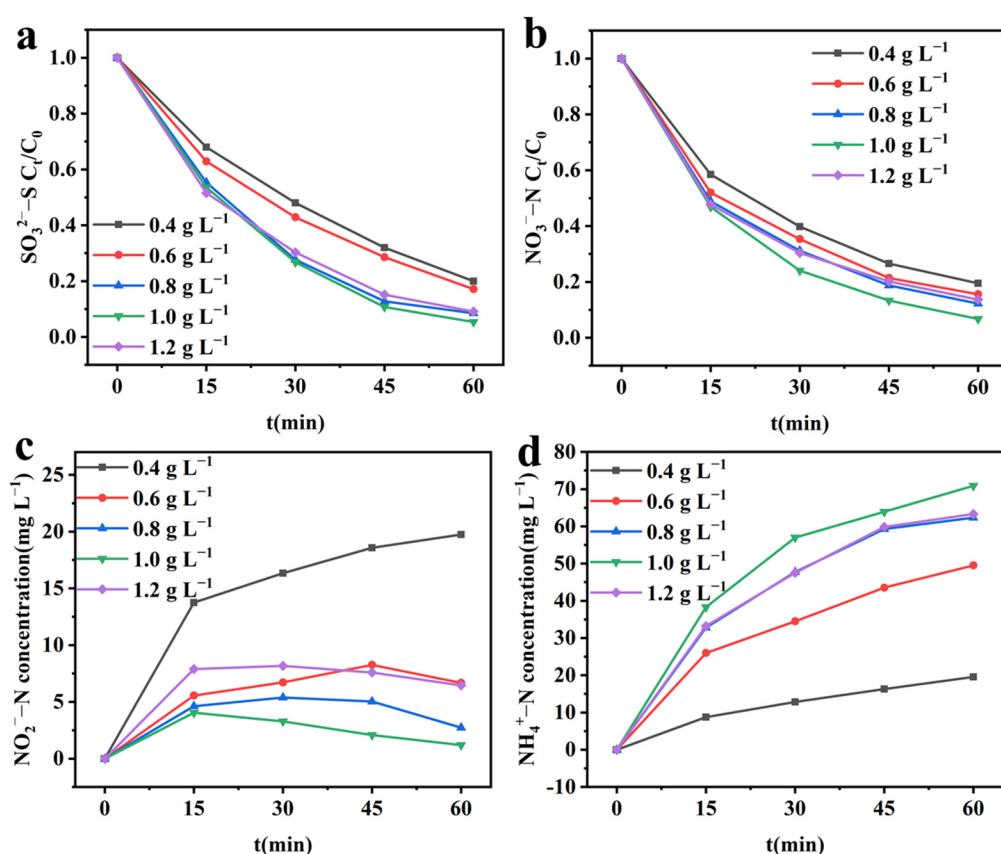


**Figure 7.** Effect of initial  $\text{SO}_3^{2-}\text{-S}$  concentration on the performance of integrated electrochemical systems. (a)  $\text{SO}_3^{2-}\text{-S}$  concentration; (b)  $\text{NO}_3^- \text{-N}$  concentration; (c)  $\text{NO}_2^- \text{-N}$  concentration; (d)  $\text{NH}_4^+ \text{-N}$  concentration. Experimental conditions: cathodic potential =  $-1.4$  V; initial  $\text{NO}_3^- \text{-N}$  concentration =  $100$   $\text{mg L}^{-1}$ .

### 3. Materials and Methods

#### 3.1. Reagents

The reagents in this work are of analytical grade or above and were used without further purification.

#### 3.2. Fabrication of $\text{CuO}\&\text{Cu}_2\text{O}\&\text{C}$ Electrode

In this study, a Pt foil ( $1\text{ cm} \times 1.5\text{ cm} \times 0.1\text{ mm}$ ) was used as the anode, and a Ag/AgCl electrode was used as the reference electrode. To investigate the accelerating effect of the SOR instead of OER, a highly  $\text{NO}_3^- \text{-RR}$ -efficient  $\text{CuO}\&\text{Cu}_2\text{O}\&\text{C}$  electrode (effective area of  $1\text{ cm} \times 1.5\text{ cm}$ ) was synthesized and used as the cathode.

The  $\text{CuO}\&\text{Cu}_2\text{O}\&\text{C}$  electrode was constructed using a redox strategy based on the previously reported research protocol with modifications [1,34]. Specifically, a carbon cloth ( $1\text{ cm} \times 2\text{ cm}$ ) was subjected to ultrasound treatment with a mixture of nitric acid (10 wt.%  $\text{HNO}_3$ ) and sulfuric acid (10 wt.%  $\text{H}_2\text{SO}_4$ ), acetone, ethanol, and deionized water for 1 h to remove surface impurities. Subsequently, 8 mL of ethylene glycol, 8 mL of ethanol, and 3 mmol  $\text{Cu}(\text{NO}_3)_2 \cdot 3\text{H}_2\text{O}$  were added to a beaker, and the mixture was thoroughly stirred for 1 h to obtain a transparent blue solution. The pretreated carbon cloth was then immersed in the solution for 4 h, and the entire system was transferred to a 25 mL hydrothermal autoclave and reacted at  $180^\circ\text{C}$  for 6 h. After the hydrothermal autoclave was cooled to room temperature, the modified carbon cloth was taken out and sonicated in anhydrous ethanol for 15 s, washed several times with water and ethanol, and dried at  $60^\circ\text{C}$  in a vacuum oven for 6 h. Finally, the modified carbon cloth was annealed in a muffle furnace at  $350^\circ\text{C}$  for 2 h to obtain the  $\text{CuO}\&\text{Cu}_2\text{O}\&\text{C}$  electrode.



conducted for 1 h. At a time interval of 15 min, 0.4 mL of solution was taken from the cathode compartment to detect the concentrations of  $\text{NO}_3^-$ -N,  $\text{NO}_2^-$ -N, and  $\text{NH}_4^+$ -N, and 1 mL of solution was taken from the anode compartment to detect the concentration of  $\text{SO}_3^{2-}$ -S. The method for the determination of ion concentrations and calculation for removal rate and selectivity were illustrated in the supporting information. Additionally, this study investigated the effects of different cathode potentials ( $-1.2$  V,  $-1.4$  V,  $-1.6$  V,  $-1.8$  V vs. Ag/AgCl), initial  $\text{NO}_3^-$ -N concentration ( $50$  mg  $\text{L}^{-1}$ ,  $100$  mg  $\text{L}^{-1}$ ,  $150$  mg  $\text{L}^{-1}$ ,  $200$  mg  $\text{L}^{-1}$ ,  $250$  mg  $\text{L}^{-1}$ ), and initial  $\text{SO}_3^{2-}$ -S concentration ( $0.4$  g  $\text{L}^{-1}$ ,  $0.6$  g  $\text{L}^{-1}$ ,  $0.8$  g  $\text{L}^{-1}$ ,  $1.0$  g  $\text{L}^{-1}$ ,  $1.2$  g  $\text{L}^{-1}$ ) on the integrated system.

#### 4. Conclusions

In summary, a cathode material for efficient electrochemical reduction of nitrate was designed, which achieved effective removal of nitrate. However, in the single reduction process, the anodic oxygen evolution reaction (OER) has certain limitations and wastes energy. Therefore, an electrochemical reduction of nitrate integrated with a sulfite oxidation system was developed. By exploring the operating parameters (cathode potential, initial nitrate concentration, and initial sulfite concentration) in the integrated system, the results show that compared with the single reduction and oxidation system, the integrated system has a faster reaction rate while achieving simultaneous treatment of harmful nitrate and sulfite. At  $-1.4$  V (vs. Ag/AgCl) cathodic potential,  $100$  mg  $\text{L}^{-1}$  initial nitrate, and  $1.0$  g  $\text{L}^{-1}$  sulfite concentrations, the nitrate removal rate and sulfite oxidation rate within 1 h reached 93.26% and 94.64%, respectively. This study provides more references for solving the mutual constraint between half-reactions.

**Supplementary Materials:** The following supporting information can be downloaded at: <https://www.mdpi.com/article/10.3390/molecules28124666/s1>, Figure S1: Fitting results of pseudo-first-order kinetic model for single electrochemical reduction of nitrate at different potentials. Figure S2. Fitting results of pseudo-first-order kinetic model for single electrochemical oxidation of sulfite at different potentials. Figure S3. Fitting results of pseudo-first-order kinetic model for integrated electrochemical system at different potentials; (a) nitrate reduction reaction; (b) sulfite oxidation reaction. Figure S4. Fitting results of pseudo-first-order kinetic model for integrated electrochemical system at different initial  $\text{NO}_3^-$ -N concentrations; (a) nitrate reduction reaction; (b) sulfite oxidation reaction. Figure S5. Fitting results of pseudo-first-order kinetic model for integrated electrochemical system at different initial  $\text{SO}_3^{2-}$ -S concentrations; (a) sulfite oxidation reaction; (b) nitrate reduction reaction.

**Author Contributions:** Conceptualization, B.C., Y.Z. and S.R.; Methodology, B.C., S.W., Y.Z. and S.R.; Validation, B.C., S.W. and X.G.; Investigation, X.G. and S.R.; Resources, Y.Z.; Writing—original draft, B.C.; Writing—review & editing, Y.Z. and S.R.; Visualization, S.W. and X.G.; Supervision, Y.Z.; Project administration, Y.Z.; Funding acquisition, Y.Z. All authors have read and agreed to the published version of the manuscript.

**Funding:** This work was funded by the Tianjin Science and Technology Project (20JCZDJC00450), Natural Science Foundation of Hebei Province (B2020202029), Central Guidance on Local Science and Technology Development Fund of Hebei Province (226Z3102G), and Fundamental Research Funds of Hebei University of Technology (JBKYTD2001).

**Institutional Review Board Statement:** Not applicable.

**Informed Consent Statement:** Not applicable.

**Data Availability Statement:** The datasets used and analyzed in the present study are available from the corresponding author upon reasonable request.

**Conflicts of Interest:** The authors declare no conflict of interest.

**Sample Availability:** Samples of the compounds are available from the authors.

## References

1. Chen, M.; Huang, X.; Wang, N.; Wang, T.; Yang, J.; Wei, Y.; Dao, X.; Zhou, L.; Hao, H. Cu<sub>2</sub>O Nanoparticles Modified BiO<sub>2-x</sub> Nanosheets for Efficient Electrochemical Reduction of Nitrate-N and Nitrobenzene from Wastewater. *Sep. Purif. Technol.* **2022**, *289*, 120728. [\[CrossRef\]](#)
2. Yao, D.; Tang, C.; Wang, P.; Cheng, H.; Jin, H.; Ding, L.X.; Qiao, S.Z. Electrocatalytic Green Ammonia Production beyond Ambient Aqueous Nitrogen Reduction. *Chem. Eng. Sci.* **2022**, *257*, 117735. [\[CrossRef\]](#)
3. Ren, T.; Ren, K.; Wang, M.; Liu, M.; Wang, Z.; Wang, H.; Li, X.; Wang, L.; Xu, Y. Concave-Convex Surface Oxide Layers over Copper Nanowires Boost Electrochemical Nitrate-to-Ammonia Conversion. *Chem. Eng. J.* **2021**, *426*, 130759. [\[CrossRef\]](#)
4. Yuan, S.; Xue, Y.; Ma, R.; Ma, Q.; Chen, Y.; Fan, J. Advances in Iron-Based Electrocatalysts for Nitrate Reduction. *Sci. Total Environ.* **2023**, *866*, 161444. [\[CrossRef\]](#)
5. Vass, Á.; Kormányos, A.; Kószó, Z.; Endrődi, B.; Janáky, C. Anode Catalysts in CO<sub>2</sub> Electrolysis: Challenges and Untapped Opportunities. *ACS Catal.* **2022**, *12*, 1037–1051. [\[CrossRef\]](#)
6. Zou, J.P.; Chen, Y.; Liu, S.S.; Xing, Q.J.; Dong, W.H.; Luo, X.B.; Dai, W.L.; Xiao, X.; Luo, J.M.; Crittenden, J. Electrochemical Oxidation and Advanced Oxidation Processes Using a 3D Hexagonal Co<sub>3</sub>O<sub>4</sub> Array Anode for 4-Nitrophenol Decomposition Coupled with Simultaneous CO<sub>2</sub> Conversion to Liquid Fuels via a Flower-like CuO Cathode. *Water Res.* **2019**, *150*, 330–339. [\[CrossRef\]](#)
7. Li, D.; Yang, J.; Lian, J.; Yan, J.; Liu, S. Recent Advances in Paired Electrolysis Coupling CO<sub>2</sub> Reduction with Alternative Oxidation Reactions. *J. Energy Chem.* **2023**, *77*, 406–419. [\[CrossRef\]](#)
8. Ali, I.; Barros de Souza, A.; De Laet, S.; Van Eyck, K.; Dewil, R. Anodic Oxidation of Sulfamethoxazole Paired to Cathodic Hydrogen Peroxide Production. *Chemosphere* **2023**, *319*, 137984. [\[CrossRef\]](#)
9. Chen, S.; Zhou, W.; Ding, Y.; Zhao, G.B.; Gao, J.H. Energy-Saving Cathodic Hydrogen Production Enabled by Anodic Oxidation of Aqueous Sodium Sulfite Solutions. *Energy Fuels* **2020**, *34*, 9058–9063. [\[CrossRef\]](#)
10. Wang, L.; Wang, J.; Xu, P.; Li, Q.; Zhang, W.; Cui, S. Selectivity of Transition Metal Catalysts in Promoting the Oxidation of Solid Sulfites in Flue Gas Desulfurization. *Appl. Catal. A Gen.* **2015**, *508*, 52–60. [\[CrossRef\]](#)
11. Wang, L.; Xing, L.; Liu, J.; Qi, T.; Zhang, S.; Ma, Y.; Ning, P. Construction of Lattice-Confined Co-MCM-48 for Boosting Sulfite Oxidation in Wet Desulfuration. *Chem. Eng. J.* **2021**, *407*, 127210. [\[CrossRef\]](#)
12. Han, J.; Cheng, H.; Zhang, L.; Fu, H.; Chen, J. Trash to Treasure: Use Flue Gas SO<sub>2</sub> to Produce H<sub>2</sub> via a Photoelectrochemical Process. *Chem. Eng. J.* **2018**, *335*, 231–235. [\[CrossRef\]](#)
13. Dubale, A.A.; Ahmed, I.N.; Zhang, Y.J.; Yang, X.L.; Xie, M.H. A Facile Strategy for Fabricating C@Cu<sub>2</sub>O/CuO Composite for Efficient Photochemical Hydrogen Production with High External Quantum Efficiency. *Appl. Surf. Sci.* **2020**, *534*, 147582. [\[CrossRef\]](#)
14. Du, F.; Cui, G.H.; Yang, B.L.; Zhang, D.S.; Song, R.F.; Li, Z.X. Ingenious Design of One Mixed-Valence Dual-Net Copper Metal-Organic Framework for Deriving Cu<sub>2</sub>O/CuO Heterojunction with Highly Electrocatalytic Performances from NO<sub>3</sub><sup>-</sup> to NH<sub>3</sub>. *J. Power Sources* **2022**, *543*, 231832. [\[CrossRef\]](#)
15. Liang, X.; Chen, X.; Xiang, Z.; Yan, R.; Xi, H.; Bian, T.; Zhang, J.; Zhao, J.; Cai, Q.; Wang, H. Design and Synthesis of Surface-Controlled CuO<sub>x</sub>/RGO Nanocomposites with Unusually High Efficiency in Catalytic Conversion of Organic Reactants in the Presence of NaBH<sub>4</sub>. *Appl. Surf. Sci.* **2018**, *459*, 716–722. [\[CrossRef\]](#)
16. Moghanlou, A.O.; Sadr, M.H.; Bezaatpour, A.; Salimi, F.; Yosefi, M. RGO/Cu<sub>2</sub>O-CuO Nanocomposite as a Visible-Light Assisted Photocatalyst for Reduction of Organic Nitro Groups to Amines. *Mol. Catal.* **2021**, *516*, 111997. [\[CrossRef\]](#)
17. Li, J.; Guo, J.; Zhang, J.; Sun, Z.; Gao, J. Surface Etching and Photodeposition Nanostructures Core-Shell Cu<sub>2</sub>O@CuO-Ag with S-Scheme Heterojunction for High Efficiency Photocatalysis. *Surf. Interfaces* **2022**, *34*, 102308. [\[CrossRef\]](#)
18. Jiang, G.; Peng, M.; Hu, L.; Ouyang, J.; Lv, X.; Yang, Z.; Liang, X.; Liu, Y.; Liu, H. Electron-Deficient Cu<sup>δ+</sup> Stabilized by Interfacial Cu–O–Al Bonding for Accelerating Electrocatalytic Nitrate Conversion. *Chem. Eng. J.* **2022**, *435*, 134853. [\[CrossRef\]](#)
19. Xu, Y.; Ren, K.; Ren, T.; Wang, M.; Wang, Z.; Li, X.; Wang, L.; Wang, H. Ultralow-Content Pd in-Situ Incorporation Mediated Hierarchical Defects in Corner-Etched Cu<sub>2</sub>O Octahedra for Enhanced Electrocatalytic Nitrate Reduction to Ammonia. *Appl. Catal. B Environ.* **2022**, *306*, 121094. [\[CrossRef\]](#)
20. He, L.; Yao, F.; Zhong, Y.; Tan, C.; Hou, K.; Pi, Z.; Chen, S.; Li, X.; Yang, Q. Achieving High-Performance Electrocatalytic Reduction of Nitrate by N-Rich Carbon-Encapsulated Ni-Cu Bimetallic Nanoparticles Supported Nickel Foam Electrode. *J. Hazard. Mater.* **2022**, *436*, 129253. [\[CrossRef\]](#)
21. Lăboşel, M.A.; Dima, G.D.; Duca, D.A.; Vaszilcsin, N.; Laurentiu Dan, M. Anodic Sulphite Oxidation on Lead Electrode in a Neutral Environment. *Mater. Today Proc.* **2022**, *78*, 302–307. [\[CrossRef\]](#)
22. Zhou, J.; Pan, F.; Yao, Q.; Zhu, Y.; Ma, H.; Niu, J.; Xie, J. Achieving Efficient and Stable Electrochemical Nitrate Removal by In-Situ Reconstruction of Cu<sub>2</sub>O/Cu Electroactive Nanocatalysts on Cu Foam. *Appl. Catal. B Environ.* **2022**, *317*, 121811. [\[CrossRef\]](#)
23. Yao, F.; Jia, M.; Yang, Q.; Chen, F.; Zhong, Y.; Chen, S.; He, L.; Pi, Z.; Hou, K.; Wang, D.; et al. Highly Selective Electrochemical Nitrate Reduction Using Copper Phosphide Self-Supported Copper Foam Electrode: Performance, Mechanism, and Application. *Water Res.* **2021**, *193*, 116881. [\[CrossRef\]](#)
24. Kong, Y.; Wang, L.; Jiang, H.; Li, F.; Zhao, T.; Zhuo, M.; Chen, Q.; Mao, M.; Xu, Y. Design of Counter Oxidation vs. CO<sub>2</sub> Electroreduction for Efficient Formate Production on a Tin Cathode. *J. Electroanal. Chem.* **2019**, *847*, 113264. [\[CrossRef\]](#)

25. Zhu, D.; Li, G.; Yan, X.; Geng, C.; Gao, L. Electrochemical Nitrate Reduction to High-Value Ammonia on Two-Dimensional Molybdenum Carbide Nanosheets for Nitrate-Containing Wastewater Upcycling. *Sci. Total Environ.* **2023**, *878*, 163145. [[CrossRef](#)]
26. Bharath, G.; Hai, A.; Rambabu, K.; Kallem, P.; Haija, M.A.; Banat, F.; Theerthagiri, J.; Choi, M.Y. Fabrication of Pd/MnFe<sub>2</sub>O<sub>4</sub> Bifunctional 2-D Nanosheets to Enhance the Yield of HCOOH from CO<sub>2</sub> Cathodic Reduction Paired with Anodic Oxidation to CH<sub>3</sub>OH. *Fuel* **2022**, *311*, 122619. [[CrossRef](#)]
27. Chen, M.; Bi, J.; Huang, X.; Wang, T.; Wang, Z.; Hao, H. Bi<sub>2</sub>O<sub>3</sub> Nanosheets Arrays In-Situ Decorated on Carbon Cloth for Efficient Electrochemical Reduction of Nitrate. *Chemosphere* **2021**, *278*, 130386. [[CrossRef](#)]
28. Fang, X.; Tan, L.; Luo, H.; Jiang, F.; Chen, H. Efficient Electrochemical Reduction of Nitrate by Bimetallic Cu-Fe Phosphide Derived from Prussian Blue Analogue. *Colloids Surf. A Physicochem. Eng. Asp.* **2023**, *658*, 130678. [[CrossRef](#)]
29. Niu, Q.; Yang, S.; Song, Z.; Liu, C.; Li, Z.; Wang, X.; Song, L. Fabrication of Efficient and Robust Fe<sup>0</sup>/Ni<sub>2</sub>P/CC Composite and the Employment for Electrochemical Reduction of Nitrate. *J. Environ. Chem. Eng.* **2021**, *9*, 106412. [[CrossRef](#)]
30. Enache, A.F.; Dan, M.L.; Muntean, R.; Vaszilcsin, N. New Electrodes Based on Pt-Co Alloys Used as Anodic Materials for Sulphite Oxidation in Alkaline Fuel Cells. *IOP Conf. Ser. Mater. Sci. Eng.* **2018**, *416*, 012072. [[CrossRef](#)]
31. Yan, X.; He, L.; Zhang, W.; Chen, W.; Wu, J.; Yang, N.; Cai, X.; Li, L.; Yan, L.; Rao, P. Efficient Ammonia-Nitrogen Removal and Recovery from Wastewater via the Continuous Flat-Sheet Gas-Permeable Membranes Reactor Pretreatment. *J. Water Process Eng.* **2023**, *52*, 103571. [[CrossRef](#)]
32. Lee, G.; Kim, K.; Chung, J.; Han, J.I. Electrochemical Ammonia Accumulation and Recovery from Ammonia-Rich Livestock Wastewater. *Chemosphere* **2021**, *270*, 128631. [[CrossRef](#)] [[PubMed](#)]
33. Chatla, A.; Almanassra, I.W.; Abushawish, A.; Laoui, T.; Alawadhi, H.; Atieh, M.A.; Ghaffour, N. Sulphate Removal from Aqueous Solutions: State-of-the-Art Technologies and Future Research Trends. *Desalination* **2023**, *558*, 116615. [[CrossRef](#)]
34. Shi, Y.; Xu, L.; Chen, M.; Yang, B.; Cheng, G.; Wu, C.e.; Miao, Z.; Wang, N.; Hu, X. Fabricating Cu<sub>2</sub>O-CuO Submicron-Cubes for Efficient Catalytic CO Oxidation: The Significant Effect of Heterojunction Interface. *J. Ind. Eng. Chem.* **2022**, *105*, 324–336. [[CrossRef](#)]

**Disclaimer/Publisher's Note:** The statements, opinions and data contained in all publications are solely those of the individual author(s) and contributor(s) and not of MDPI and/or the editor(s). MDPI and/or the editor(s) disclaim responsibility for any injury to people or property resulting from any ideas, methods, instructions or products referred to in the content.